Electron Bernstein Emission characterization in TJ-II

J. M. García-Regaña[1], A. Cappa [1], F. Castejón[1], J. B. O. Caughman[2] and M. Tereshchenko[3,4]

[1]*Laboratorio Nacional de Fusión, EURATOM-CIEMAT, Madrid, Spain*
[2]*Oak Ridge National Laboratory, Oak Ridge, TN USA*
[3]*BIFI: Instituto de Biocomputación y Física de Sistemas Complejos, Zaragoza, Spain*
[4]*Prokhorov Institute of General Physics, Moscow, Russia*

Introduction: the EBWH and EBE systems

Taking advantage of the installation of an Electron Bernstein Wave Heating (EBWH) system in the TJ-II Stellarator, (O-X-B mode conversion at 1st harmonic, 28 GHz, and 300 kW of available power), an Electron Bernstein Emission (EBE) diagnostic that uses the internal mirror of the EBWH system, was installed (28 GHz heterodyne radiometer dual polarized) [1]. Its aim is to determine the optimal (maximum O-X conversion efficiency η) launching direction for heating by finding the line of sight that measures the maximum intensity of B-X-O-converted radiation. In the present work the analysis of the emission signal obtained by performing a scan of the mirror position is compared with the numerical results carried out with the TRUBA [2] code as multi-ray tracer. The experimental determination of the polarization of the received signal is also studied. In figure 1 the layout of the EBWH and EBE systems is schematically represented. The mirror that determines the launching direction also collects the EBE radiation and redirects it to the radiometer. The launching direction is defined by a pair of positioning angles $(\alpha_\phi, \alpha_\theta)$, while the radiation collected by the mirror along that line is redirected to the EBE radiometer by shifting the mirror position by a primed pair $(\alpha'_\phi, \alpha'_\theta)$. For notation convenience the primes will be removed for the remainder of the text. The quad ridge dual polarized horn measures the 28 GHz radiation along two orthogonal directions. This set-up allows to determine experimentally the polarization of the received radiation by rotating the top of the diagnostic. The rotation angle is denoted by ζ.

Numerical and experimental EBE window: $I_{\mathrm{EBE}}(\alpha_\phi, \alpha_\theta)$

The numerical results are obtained by launching multiple rays for the beam simulation. The beam characteristics are defined by the steerable mirror design [3]. The beam width at the waist is $2w_0 = 0.06$ m, and the distance from the center of the mirror to the waist is $z_0 = 0.3$ m. Thus, a Gaussian weighting factor g_i is considered for every ray. The i subindex corresponds to the i-th ray. The TRUBA code also provides the conversion efficiency η_i according to the one dimensional O-mode tunneling theory. Once the converted rays have been traced the well-

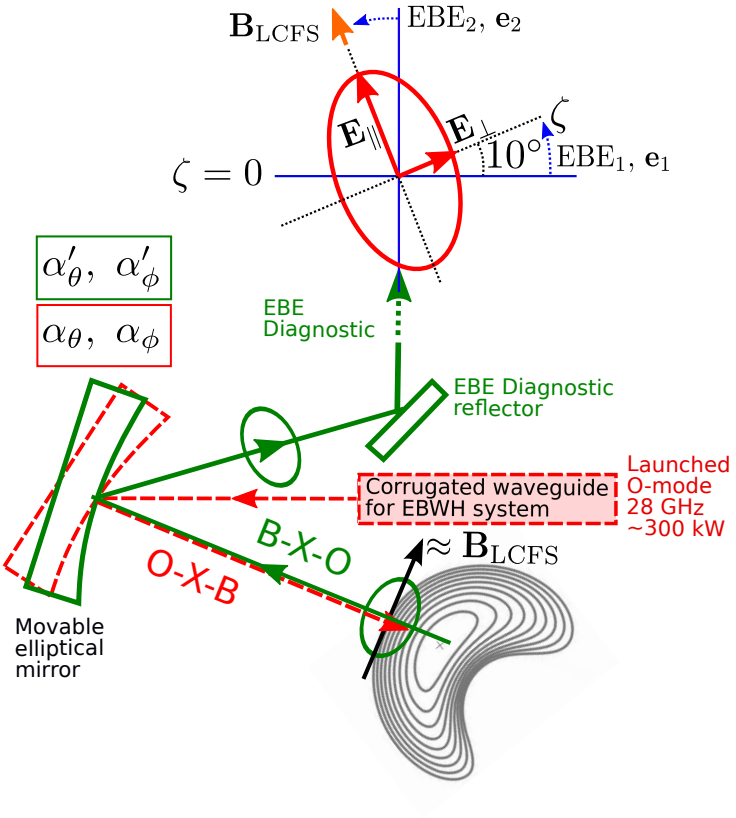

FIGURE 1: Schematic view of the EBWH system and the EBE diagnostic. The theoretical polarization of the detected B-X-O-converted radiation projected on the detection plane is shown in the top of the figure. $\mathbf{E}_{\parallel}$ and $\mathbf{E}_{\perp}$ are the parallel and perpendicular electric field referred to the magnetic field at the LCFS, $\mathbf{B}_{\mathrm{LCFS}}$. When the rotation angle of the EBE diagnostic is $\zeta = 0$, the direction of the channels EBE_1 and EBE_2 are coincident with the polarization vectors $\mathbf{e}_1$ and $\mathbf{e}_2$. For $\zeta = 10$, the two channels are aligned with the axis of the expected polarization ellipse.

known integral for the intensity emerging from the plasma,

$$I_\omega = \frac{\omega^2}{8\pi^3 c^2} \int_0^{\tau_0} T \mathrm{e}^{-\tau} \mathrm{d}\tau, \tag{1}$$

is performed up to the tunneling point, providing a value of intensity for each ray I_i. The total EBE intensity emerging from the plasma, I_{EBE}, results from summing the contribution of the n_c converted rays multiplied by the corresponding weighting factors g_i and η_i

$$I_{\mathrm{EBE}} = \sum_i^{n_c} \eta_i g_i I_i. \tag{2}$$

Figure 2(a) shows the map of the total conversion efficiency of the beam η. Figure 2(b) shows the sum of the EBE intensity up to the tunneling point, i.e. removing the factor η_i from eq. 2. Finally 2(c) shows I_{EBE} as defined in eq. 2. The similar shape of maps 2(a) and 2(c) justifies the usage of the EBE radiation as diagnostic for the conversion efficiency η.

The experimental data are obtained by summing up the signals of the two EBE channels at the TS acquisition time, once the overdenseness condition is fulfilled during the NBI heating phase. Each measurement belongs to a different TJ-II shot, and a strong variability in the T_e profile can be obtained from one shot to another. To overcome this lack of reproducibility, the strong dependence of I_{EBE} on the temperature is eliminated by normalizing its value to the electron temperature at the plasma center.

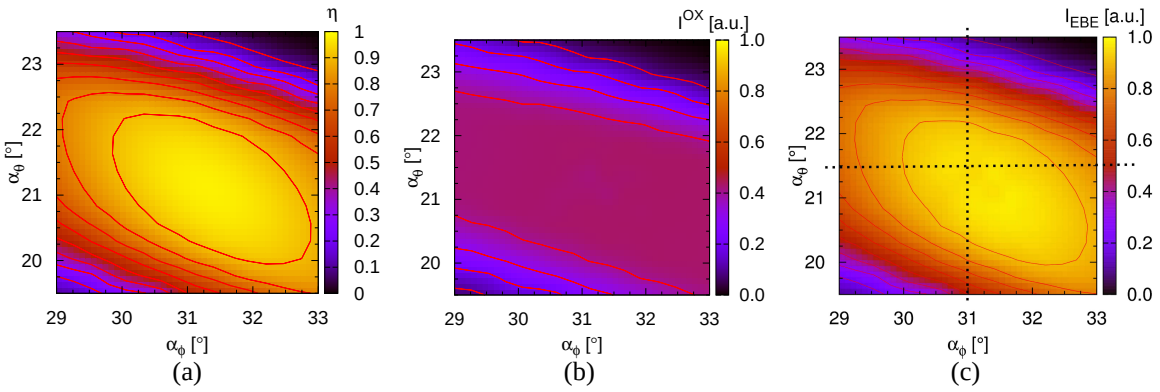

FIGURE 2: 2(a) O-X conversion efficiency (η) as a function $(\alpha_\phi, \alpha_\theta)$. 2(b) Map of EBE radiation reaching the O-X conversion layer, i.e. before suffering the X-O conversion. 2(c) EBE radiation leaving the plasma after X-O conversion, i.e. applying formula 2 for I_{EBE}. The dotted lines represented the experimental scans performed. The central electron temperature and density values are 0.3 keV and $n_0 = 3.5 \times 10^{19}$ m^{-3}. The profiles are fitted to the TS profiles by the expressions: $n_e(\rho) = n_0(1-(\rho^2)^{1.6})^{2.7}$ and $T_e(\rho) = T_0(1-(\rho^2)^2)^{1.7}$.

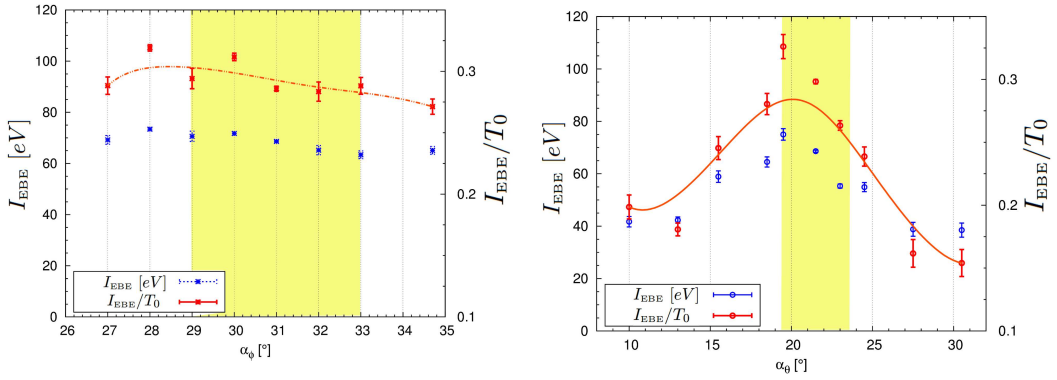

FIGURE 3: 3(a)I_{EBE} dependence on α_ϕ for $\alpha_\theta = 21.5°$. 3(b) I_{EBE} dependence on α_θ for $\alpha_\phi = 31°$. The shadowed area corresponds to the interval in α_θ and α_ϕ represented in figures 2(a)-2(c)

The experimental results were obtained by scanning α_ϕ at a fixed value of the poloidal angle $\alpha_\phi = 21.5°$, and scanning α_θ, for a fixed value of $\alpha_\phi = 31°$. The results from this scans are shown in figs. 3(a) and 3(b) respectively. Comparing the former figure with 2(c) it can be observed that the maximum experimental value of I_{EBE} is displaced to the left side of the α_ϕ domain. In respect to the poloidal scan, the theoretical maximum is located around $\alpha_\theta \approx 21°$ while the experimental one is in $\alpha_\theta \approx 19.5°$. This represents a noticeable deviation due to the narrowness of the EBE window along that direction. Furthermore, the values at the boundaries of the α_θ domain shows a large contribution of disperse radiation.

The EBE polarization

A scan in the rotation angle ζ has been performed in order to verify that the measured radiation comes from a B-X-O conversion process. During this scan, we measure the ratio between

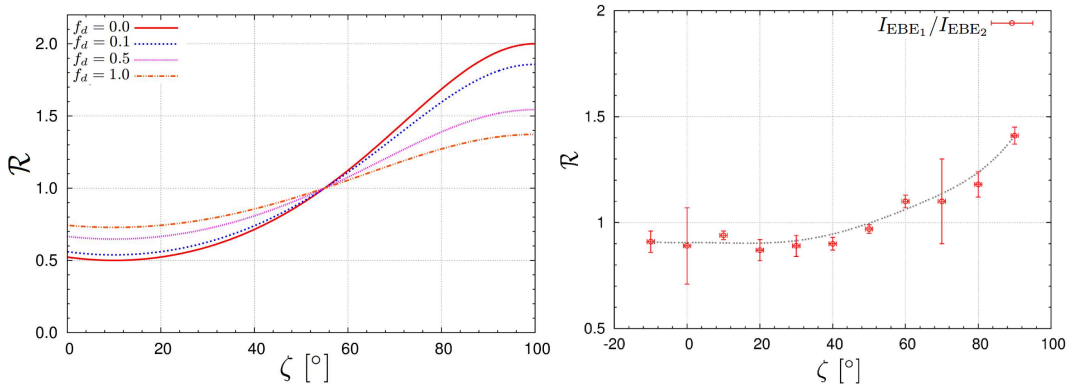

(a) (b)

FIGURE 4: 4(a)Theoretical estimation of $\mathscr{R}$ as function of ζ for different fractions of disperse radiation (f_d). 4(b) Experimentally measured ratio between the intensity reaching every EBE channels, $\mathscr{R}(\zeta)$.

the signals from each channel or the power dissipated by the electric field along the detection directions: $\mathscr{R}(\zeta) = I_{\text{EBE1}}(\zeta)/I_{\text{EBE1}}(\zeta) = P_1(\zeta)/P_2(\zeta)$. It can be shown that $\mathscr{R}(\zeta)$ is shaped as fig. 4(a) represents. The figure shows the power ratio $\mathscr{R}$ with and without considering a fraction f_d of disperse radiation with respect to the maximum power that the channel EBE_1 would receive: $P_d = f_d P_1(\zeta = 10°)$. Thus, the power ratio $\mathscr{R}$ is simply modified by the disperse radiation as

$$\mathscr{R}(\zeta) = \frac{P_1 + P_d}{P_1 + P_d}. \tag{3}$$

The experimental scan on ζ was performed at the position $(\alpha_\phi, \alpha_\theta) = (31°, 19.5°)$, and the result is shown in figure 4(b). Comparing it with fig. 4(a) it can be concluded that the measured radiation is consistent with an O-mode polarization, although remarkably screened by the disperse radiation.

Conclusions

In this work the EBE radiation has been successfully applied for diagnosing the O-X conversion efficiency. This usage has been numerically demonstrated and experimentally verified. In the limited explored region, the results have shown an appreciable deviation between the numerical and experimental EBE window in TJ-II, and have demonstrated that a non negligible fraction of the detected radiation comes from the B-X-O conversion mechanism. A fine scan of the EBE window and the polarization at different positions are necessary for a complete characterization of the O-X conversion problem in TJ-II.

References

[1] J. B. O. Caughman *et. al. Fusion Science and Technol.* **57** 1, 41 (2010)
[2] M. A. Tereshchenko *et al Proceedings of the 30th EPS Conference on Contr. Fusion and Plasma Phys.* **27A** P-1.18 (2003)
[3] F. Castejón *et. al.*, *Nucl. Fusion* **48**, 075011 (2008)